Aging and Disease
www.aginganddisease.org
Early access date: January 14, 2025
http://dx.doi.org/10.14336/AD.2024.1654

Original Article

NR1D1 Inhibition Enhances Autophagy and Mitophagy in Alzheimer's Disease Models

Shi-qi Zhang[1#], Zhangming Niu[2, 3, 4#], Alexander Anisimov[1], Fang Shi[5], Shenglong Deng[2], Xianglu Xiao[2, 3, 6], Shu-qin Cao[1], Jun-ping Pan[1], He-Ling Wang[1], Maria J. Lagartos-Donate[1], Nihal Gullu Bozbas[7], Ping-Jie Wang[8], Ruixue Ai[1], Yan Li[9], Guang Yang[6, 4, 10, 11*], Sofie Lautrup[1*], Evandro F. Fang[1, 12*]

[1]Department of Clinical Molecular Biology, University of Oslo and Akershus University Hospital, Lørenskog 1478, Norway. [2]Mindrank AI Ltd, Hangzhou, China. [3]AI Research Center, MindRank Technologies Limited, London, UK. [4]National Heart and Lung institute, imperial college London, London, SW7 2AZ, UK. [5]Guangzhou Key Laboratory of Formula-Pattern of Traditional Chinese Medicine, School of Traditional Chinese Medicine, Jinan University, Guangzhou 510632, China. [6]Bioengineering Department and Imperial-X, Imperial College London, London, W12 7SL, UK. [7]Faculty of Medicine, Acibadem University, Istanbul, Turkey. [8]Department of Neurrology, The First Affiliated Hospital, Zhengzhou University, Zhengzhou, China. [9]Formula-Pattern Research Center, School of Traditional Chinese Medicine, Jinan University, Guangzhou, China. [10]Cardiovascular Research Centre, Royal Brompton Hospital, SW7 2AZ London, United Kingdom. [11]School of Biomedical Engineering & Imaging Sciences, King's College London, London, United Kingdom. [12]The Norwegian Centre on Healthy Ageing (NO-Age) and the Norwegian National Anti-Alzheimer's Disease (NO-AD) Networks, Oslo, Norway.

[Received December 13, 2024; Revised January 7, 2025; Accepted January 8, 2025]

ABSTRACT: Alzheimer's disease (AD) is marked by extracellular beta-amyloid (Aβ) plaques and intracellular Tau tangles, leading to progressive cognitive decline and neuronal dysfunction. Impaired autophagy, a process by which a cell breaks down and destroys damaged or abnormal proteins and other substances, contributes to AD progression. This study investigated Nuclear Receptor Subfamily 1 Group D Member 1 (NR1D1) as a potential therapeutic target for modulating autophagy. We show that NR1D1 depletion significantly enhances autophagic flux and mitophagy in human cell lines as well as wildtype and AD *Caenorhabditis elegans* (*C. elegans*) models. Our findings revealed that *NR1D1* knockdown increased autophagy markers and activated the proteins Sirtuin 1 (SIRT1) and CTSB cathepsin B (Cathepsin B), both linked to autophagy function. In 5 familial AD mutations (5xFAD) mice, *Nr1d1* knockdown restored the expression level of autophagy markers. *C. elegans* experiments revealed that depletion of the worm ortholog of *NR1D1, nhr-85,* improved neuronal mitophagy, enhanced associative memory in amyloid-β models, and extended lifespan. These findings suggest NR1D1 as a promising therapeutic target for improving cellular autophagy mechanisms in AD.

Key words: NR1D1, autophagy, mitophagy, Alzheimer's disease

INTRODUCTION

Nuclear receptor subfamily 1 group D member 1 (NR1D1), also known as Rev-erbα, is a member of the nuclear receptor family that is highly expressed in multiple organs of humans and other mammals [1, 2]. NR1D1 plays a role in numerous mechanisms in the human body, including circadian rhythm, metabolism, inflammation, apoptosis, and autophagy [3-8]. Autophagy, a cellular process that degrades and recycles damaged organelles, misfolded proteins, and other cellular debris through lysosomal pathways plays important roles in various diseases and aging. *Nr1d1* knockout has been shown to markedly increase

***Correspondence should be addressed to:** Dr. Guang Yang, Bioengineering Department and Imperial-X, Imperial College London, London, W12 7SL, UK. Email: g.yang@imperial.ac.uk. Dr. Sofie Lautrup, University of Oslo and Akershus University Hospital, Lørenskog 1478, Norway. Email: s.h.lautrup@medisin.uio.no. Dr. Evandro F. Fang, University of Oslo and Akershus University Hospital, Lørenskog 1478, Norway. Email: e.f.fang@medisin.uio.no. #These authors contributed equally.

autophagy, including mitochondrial autophagy, in certain cancers. Loss of NR1D1 hereby led to energy dyshomeostasis and increased oxidative stress [9, 10]. Additionally, activation of NR1D1 has been found to inhibit autophagy, thereby reducing cancer cell proliferation and migration [11]. Combined, previous studies suggest that NR1D1 serves as a significant upstream regulator of autophagy, however, the precise mechanisms by which NR1D1 regulates autophagy remain unclear and warrant further investigation.

Alzheimer's disease (AD) is a neurodegenerative disorder characterized by amyloid plaques and tau tangles [12, 13]. Autophagy declines with aging and in AD, contributing to the accumulation of pathological proteins, such as Amyloid β (Aβ) and tau [14-16]. Enhancing autophagy has been shown to decrease AD symptoms, whereas compromised autophagy exacerbates amyloidosis and tau pathology during AD progression [17, 18]. Additionally, mitochondrial damage and associated energy metabolism dyshomeostasis are hallmarks of AD and hold promise as novel therapeutic targets for AD [19, 20]. We recently reported that mitophagy, mitochondrial-specific autophagy, is impaired in AD, resulting in an accumulation of damaged mitochondria in the AD brain [21, 22]. Drugs specifically targeting mitophagy have been demonstrated to alleviate AD-related pathologies and to improve memory and learning abilities of AD animal models [21, 22]. Overall, targeting autophagy and mitophagy represents a promising strategy for AD treatment.

In this study, we examined the potential of NR1D1 as a target for future AD-drugs, based on its negative association with autophagy. We demonstrated that *NR1D1* knockdown led to enhanced autophagy in both cells and *C. elegans*. This finding prompted us to investigate NR1D1 as a regulatory target for autophagy in diseases characterized by autophagy defects, such as AD. Maintaining a balance between autophagy and mitophagy is crucial in daily life; however, in autophagy-deficient and AD-affected conditions, enhancing autophagy by modulating NR1D1 may provide a novel therapeutic approach for AD and other autophagy-related disorders.

METHOD AND MATERIAL

C.elegans: Short-term memory assay

Chemotaxis to volatile compounds were performed at 20 °C, on agar plates as described previously [21, 23]. First, around 200-300 synchronized day-1 worms were collected and washed with M9 buffer 5 times, followed by placing them on plain 6 cm NGM plates (without OP50) with or without IA for 120 mins. In the IA conditioning group, 10 µl pure IA was placed inside the lid in the middle. 30 mins before transferring the worms, assay plates were prepared. 20 µl of 20 mM NaN3 was added to 'IA' and 'T'/'trap' points, respectively. Left at room temperature (20-22 °C) for 30 mins, the assay plates were dry enough for testing. Then the 'IA' area was covered with a 0.5x0.5 cm piece of Parafilm. After 120 mins, worms were collected by M9 buffer, followed by placing the worms on the 'source point' area (quickly dried worms via tissue paper). 4 µl of diluted IA (1/50) was added to the Parafilm. The testing plates then were quickly sealed by parafilm. After training for 120 mins, the number of worms in regions of 'source point/S', 'IA', and 'T' were counted. The chemotaxis index was (#'IA' - #'T')/(#'IA' + # 'T' + #'S'), where '#' denotes numbers. Better memory performance correlates with a smaller score.

C.elegans: Lifespan assay

The lifespan assay was conducted at 20°C using 6 cm diameter NGM plates with a lawn of OP50, as previously described [21]. The different strains of worms (Supplement Table 3) were divided into two groups from egg stage: control and *nhr-85* RNAi. Synchronous animals were generated through bleaching-defined conditions. Day-0 worms (L4 stage) were transferred to 6 cm plates with FUDR treatment, approximately 30-35 per technical repeat. Three technical repeats were conducted per biological repeat. In total, two biological repeats were performed on three different days. In first 8 days after the adult stage of worms, the plates were renewed every 4 days to maintain consistent drug exposure. Daily assessments were conducted to categorize worms as either alive or deceased. Worms were classified as dead if they exhibited a cessation of pharyngeal pumping and were unresponsive to touch. Instances where worms died due to gonad extrusion, internal bagging, or crawling along the plate's periphery were annotated as censored. Censored cases were assigned a weight of '0' in the calculations for mortality.

Evaluation of neuronal mitophagy inducers using a C. elegans mitophagy reporter strain

To evaluate mitophagy activity in wildtype and Alzheimer's animal models, a previously described pan-neuronal mitophagy reporter strain of *C. elegans* (neuronal mt-Rosella) was used and crossed with TU3401 strain [21]. These worms express a pan-neuronal mt-Rosella biosensor, which is a fusion protein composed of a variant of GFP, sensitive to the acidic environment of the lysosomal lumen, and the Discosoma red fluorescent protein (DsRed) pH-insensitive [24]. Mitophagy activity event were calculated as the ratio between the number of pixels for GFP and DsRed (GFP/DsRed). Thus, lower

values of the ratio correlate with lower mitophagy activity, and vice versa. For all nematode experiments, RNAi bacteria were administered from egg stage onwards. The images of the worms were taken on day 1 by using a Fluorescence microscope (Nikon TI-BDTV2 inverted microscope).

Cell culture

YFP-Parkin HeLa (YPH) and HeLa monomeric Keima (mt-Keima) cells were a gift from Prof. Hanming Shen and Dr. Lu Guang at the National University of Singapore (Singapore). U2OS WT cell was a gift from Dr. Nuo Sun. Microtubule-associated protein 1 light chain 3 (LC3) fused to mRFP and EGFP U2OS cell line was a gift from Prof. Anna Simonson at the University of Oslo (Norway). U2OS Cells were cultured and maintained in DMEM with 4.5g/L glucose with L-gln, without sodium pyruvate (cat. No 41965062, Gibco, United States), and supplemented with 10% FBS (cat. No 10270106, Gibco, United States) and 1% Penicilin-Streptomycin (P&S) in the humidified incubator (37°C, 5% CO2). The culture medium was changed every 2 to 3 days. Cells were used for future experiments when they reach 80 to 90% confluence.

NR1D1-siRNA experiment in cell line

siRNA was obtained from OriGene (cat. No SR322830). The siRNA or scrambled (Scr) control siRNA Oligo Duplexes at 20nM and 40 nM were transfected using Lipofectamine® RNAiMAX (cat. No 13778150, Invitrogen, ThermoFisher, USA) following the standard protocol. For each transfection, 6 µl of Lipofectamine® RNAiMAX and 20-40 nM of the siRNA were added to 200 µl of Opti-MEM (cat. No 31985070, Invitrogen, United States) and incubated for 10 minutes at room temperature. The mixture was then added to the cells, bringing the total volume to 1 ml, and incubated for 4-6 hours. Subsequently, 1 ml of 20% serum culture medium was added to achieve a final serum concentration of 10%. The medium was changed to normal 10% serum medium after 24 hours. After 48 hours post-transfection, the cells were collected for various experimental purposes. Western blot analysis was employed to assess knock-down efficiency.

Cell Viability

3-(4,5-Dimethylthiazol-2-yl)-2,5-diphenyl tetrazolium bromide (MTT) is a widely used chemical indicator for cellular metabolic activity and cell viability based on the ability of nicotinamide adenine dinucleotide phosphate (NADPH)–dependent cellular oxidoreductase enzymes which reduce the yellow MTT to purple formazan in living cells. The formazan redissolved in the solubilization solution such as DMSO and provides a colorimetric assay. In this study, MTT was used to detect cell viability for both YPH and U2OS cells. 3000-5000 cells were seeded and grown in each well of 96-well plates overnight in a humidified 5% CO2 incubator at 37 °C. Next day, the cells were knocked down using siRNA or empty vector. After knockdown, cells were exposed to MTT for 3 h. Then, all supernatant was removed, and the formazan crystals were dissolved with DMSO (200 µL) before measuring the absorbance at 550 nm.

Quantification of cellular mitophagy using HeLa mt-Keima cells

The HeLa Parkin mt-Keima cells (25,000 cells/well) were seeded in 35mm µ-Dish (IB81156, ibidi, United States) applying knockdown. After knockdown, the medium would be treated with FCCP (30µM) or same volume DMSO and followed by 6h incubation. Finally, cells were imaged using confocal microscope (ZEISS, LSM780) under excitation at 458nm for green and 586 nm for red channel, respectively; and emission at 570-695 nm. Images were then analyzed using Image J software.

Detection of Mitochondrial Membrane Potential in Live Cells

The mitochondrial membrane potential in live cells was assessed using TMRE (cat. No T669, Invitrogen, ThermoFisher, USA), a cell-permeant fluorescent indicator that selectively accumulates in active mitochondria, emitting a bright fluorescent signal. YPH cells were pretreated FCCP (20 µM for 6 hours) or same volume of DMSO. Following treatment, cells were stained with TMRE (100 µM) and Hoechst 33342 (2 µg/mL) for 15 minutes in the dark and wash two times. After staining, cells were washed with warm medium and imaged using a confocal microscope (ZEISS, LSM780) at 63× magnification. Simultaneously, cells were cultured in 96-well plates and subjected to the same treatment protocol. Prior to measurement, PBS was used to replace the culture medium to prevent interference from Phenol Red. Fluorescence detection was performed using an ELISA reader with an excitation peak at 549 nm and an emission peak at 574 nm. Following this, PBS was replaced with culture medium, and an MTT assay was conducted to evaluate cell viability under different conditions. The TMRE fluorescence values were normalized against the MTT-derived cell viability values, and the standardized results were subjected to statistical analysis.

Mitochondrial Morphometrics Analysis

Following knockdown in YPH cells, the cells were treated with either FCCP (20 μM for 6 hours) or same volume of DMSO. Cells were exposed to 200 nM Red MitoTracker (cat. No M22425, Invitrogen, USA) and Hoechst 33342 (2 μg/mL) for 30 minutes. After staining, cells were washed twice with PBS and immediately examined using confocal microscopy (ZEISS, LSM780) at 63× magnification. The relative red fluorescence intensity was quantified using the ImageJ Mitochondria Analyzer.

Tracking of Acidic Lysosome

Following knockdown in YPH cells, the cells were treated with either Baf-A1 (100 nM for 2 hours) or same volume of DMSO, EBSS 2 hours. Cells were exposed to 75 nM Red LysoTracker (cat. No L7528, Invitrogen, USA) and Hoechst 33342 (2 μg/mL) for 30 minutes. After staining, cells were washed twice with PBS and immediately examined using confocal microscopy (ZEISS, LSM780) at 63× magnification. The relative red fluorescence intensity was quantified using ImageJ.

Western blot analysis using materials from cell, mouse brain and Human brain

Samples from cells and mouse brain were gathered and lysed using 1x radioimmunoprecipitation assay (RIPA, catalog no. 89901, Thermo Scientific, USA) buffer containing protease and phosphatase inhibitors (catalog no. 78445, Thermo Scientific, USA), incubate the samples on the ice for 30 minutes. After centrifugation at 13,300 × RPM at 4°C for 30 minutes. The normalized supernatant was collected and denatured at 95°C for 5 minutes with 4xLDS loading dye (catalog no. NP0008, Invitrogen, USA). Protein concentration was determined using the BSA method. NuPAGE 4-12% Bis-Tris Protein Gel (catalog no. MP41G15, sigma-Aldrich, USA) was utilized for protein separation, run at 150V for 45 minutes. The transfer system was set at 250mA for 1~3 hours on a PVDF membrane (for proteins ranging from 15 kDa to 350 kDa). To prevent non-specific binding, 5% BSA dissolved in Tris-HCl buffer containing 0.1% Tween-20 was used for blocking.

Blots were then incubated with primary antibodies and 24 hours later they were washed (three washes of 10 minutes each) and incubated with the secondary antibodies conjugated to horseradish peroxidase (HRP) for 2 hours. Afterwards, another three washes were conducted. Immediately after the chemiluminescence was detected using the ChemiDoc XRS System (Bio-Rad Laboratories), and quantification was performed using ImageJ. The primary antibodies and secondary antibodies used for this experiment were in the following form. Primary antibodies were used at a 1:1000 dilution, with secondary antibodies used at a 1:5000 dilution (Table 1).

Table 1. The list of antiblodies.

Antibody	Brand	Cat no.
mTOR	Cell Signalling technology	2983S
LAMP2	Cell Signalling technology	34141S
ULK1	Cell Signalling technology	6439S
SIRT1	Cell Signalling technology	9475S
TFEB	Cell Signalling technology	37785S
HSP90	Cell Signalling technology	4874S
Beclin-1	Cell Signalling technology	3495S
NAMPT	Cell Signalling technology	61122
ATG5	Cell Signalling technology	12994S
GAPDH	Cell Signalling technology	2118S
Cathepsin D	Abcam	ab6313
Cathepsin B	Cell Signalling technology	31718S
LC3B	Cell Signalling technology	43566S
beta Actin	Invitrogen	PA5-72633
p62	Cell Signalling technology	39749S
NR1D1/Rev-Erbα	Cell Signaling Technology	13418

Transgenic mice: Ethics

All animal procedures were approved by the Jinan University Institutional Animal Care and Use Committee. All animals were maintained at the Jinan University Institutional Animal Care Facility under standard conditions under 12h-12h light–dark cycle. All animal procedures were approved by the Jinan University Institutional Animal Care and Use Committee (IACUC-20231115-02).

Virus information

All viral tools used in behavioral experiments of hTau.P301S mice were provided and packaged in BrainVTA (BrainVTA Co., Wuhan, China). The adeno-associated viruses (AAVs), PT-9634 rAAV-CX3CR1-EGFP-S'miR-30a-shRNA2(*Nr1d1*)-3'miR-30a-WPREs and PT-2961 rAAV-CX3CR1-EGFP-5'miR-30a-shRNA(*scramble*)-3'miR-30a-WPREs were packaged into AAV2/6 serotypes with final titers at least 2×10^{12} genome copies per milliliter.

Surgery and viral injections

For the 7-month-old 5xFAD mice, the mice were first anesthetized with 10% ethyl urethane, 2% chloral hydrate, and 1.7 mg/mL xylazine in a 0.9% NaCl mixture (0.09 ml/10 g body weight, i.p.). Then the mice were mounted in a stereotaxic holder (item: 71000, RWD, Shenzhen, China). The experimental mice skulls were adjusted to be parallel to the reference panel. A dental drill was used to

make a craniotomy (~0.5 mm diameter) above the target areas. 0.5 μL was microinjected (coordinates were AP: ~0.2 mm from the posterior transverse sinus as measured 4 mm lateral to the midsagittal sinus, ML: 0,2 mm from midsagittal sinus, depth: ~1–1.5 mm). 15 days were required to be adequate for the AAV expression. After virus injection for 2 months, the 9-month-old mice were applied to the sacrifice and tissue collection.

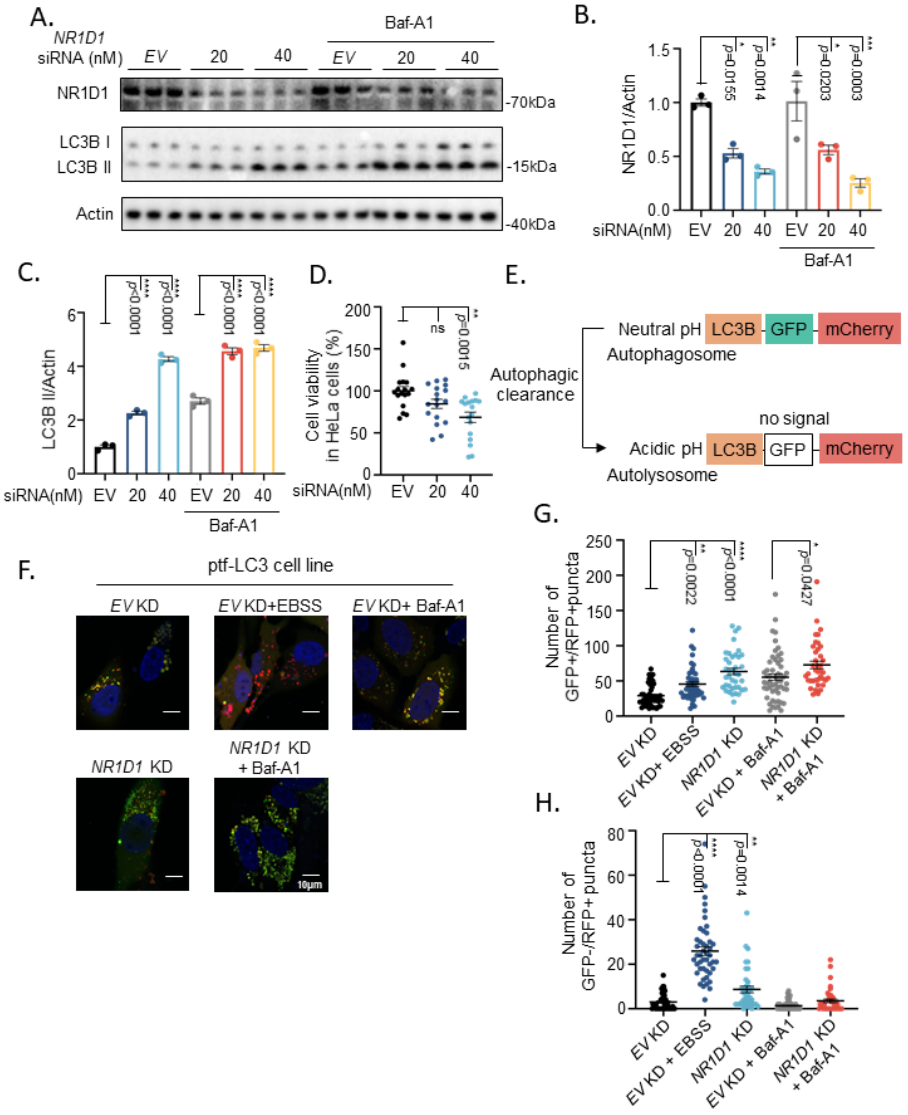

Figure 1. NR1D1 as a Negative Regulator of Autophagy. (A) Western blot detection of NR1D1, p62, LC3B, and Actin protein expression levels in YFP-Parkin-HeLa (YPH) cells treated with *empty vector* (*EV*) or NR1D1 siRNA (20nM and 40nM) with or without Baf-A1 treatment, showing the knockdown efficiency of *NR1D1* siRNA and its impact on autophagy-related proteins. Data are pooled from 3 biological replicates (n=3). **(B, C)** Quantification of NR1D1 (B) and LC3B II (C) protein levels in cells treated with EV or *NR1D1* siRNA at different concentrations in YPH cells treated with *EV* or *NR1D1* siRNA (20nM and 40nM) with or without Baf-A1 treatment. **(D)** MTT assay in HeLa cells treated with *EV* or *NR1D1* siRNA in YPH to detect the cell viabiliy. Data are pooled from 3 biological replicates and each repeat contains 5-6 technical repeats (n=17). **(E)** Schematic representation of autophagosome and autolysosome formation, highlighting the fluorescence of GFP-mCherry-LC3B in neutral and acidic conditions. **(F)** Representative images of puncta in ptf-LC3B cells treated with *EV* KD, EBSS, *NR1D1* KD, or *NR1D1* KD with Baf-A1. Data are pooled from 3 biological replicates and each repeat contains 8 pictures per group. The result quantified the result by single cell per group (n=39-54). **(G, H)** Quantification of the number of GFP+RFP+ puncta (G) and GFP- RFP+ puncta (H), representing specific autophagic stages. Two-way ANOVA with Tukey's multiple comparison test (B, C, G, H) and Kruskal–Wallis test with Dunn's multiple comparison test (D) were performed for statistical analysis, with significance levels denoted as follows: ns = not significant, * $p < 0.05$, ** $p < 0.01$, *** $p < 0.001$, **** $p < 0.0001$. All data are presented as mean ± SEM.

ROSMAP single-nucleus RNA-seq data analysis

The analysis presented here utilized data from the ROSMAP cohort, accessible through the AD Knowledge Portal. We acknowledge their contributions to generating and sharing the data used in this research. The details of preprocessing, quality control, and cell type annotation steps can be found in their recent paper [25]. We extracted the raw data from the cell type objects available in the synapse platform to perform differential analysis.

Statistical analyses

In the result section, relative expression level is the level of genes/proteins in a group compared to the level in designated WT (or other control). The Shapiro-Wilk test (that determines normality when $n \geq 6$) was used first to determine whether the data deviated from Gaussian distributions. We performed a Shapiro-Wilk test to check for normal Gaussian distribution. If the data followed a normal distribution, we used Tukey's multiple comparisons tests for one-way/two-way ANOVA. If the data did not follow a normal distribution, we used the Kruskal-Walli's test, followed by Dunn's multiple comparisons. For smaller sample sizes ($n<6$), we conducted non-parametric tests using the Wilcoxon test. T-tests and one-way/two-way ANOVA were applied to compare two independent groups and three or more groups, respectively. The data are presented as the means ± standard errors of the means (SEMs), and differences were considered statistically significant when $p < 0.05$.

RESULTS

NR1D1 Inhibition Enhances Autophagic Flux

Previous studies have suggested a link between NR1D1 inhibition and activation of autophagy [11, 26]. To further validate whether NR1D1 suppression activates autophagy and enhances autophagic flux in human cells, we employed a HeLa cell line overexpressing Parkin tagged with yellow fluorescent protein (YFP), since HeLa cells lack endogenous Parkin expression [27], and confirmed our results in wildtype U2OS cells. We performed siRNA-mediated knockdown of *NR1D1* using increasing concentrations of the siRNA in both YPH and U2OS cells, to investigate the dose-dependent relationship between NR1D1 expression and autophagy activation through LC3B and sequestosome-1 (p62) detection using Western Blotting (Fig. 1 A-C; Supplementary Fig. 1A-F). LC3B is often used as a marker for autophagy. Upon autophagy activation LC3B I is converted to LC3B II via lipidation, which facilitates the association of LC3B II to the autophagosome membrane where it facilitates autophagosome formation and autophagy progression. Additionally, we employed Bafilomycin A1 (Baf-A1) to block autophagosome-lysosome fusion, enabling assessment of autophagic flux [28]. Baf-A1 treatment prevents the degradation of autophagosomes by inhibiting lysosomal acidification, allowing their accumulation to be measured as an indicator of autophagic flux. Baf-A1 causes an accumulation of LC3B II-tagged autophagosomes, enhancing the detection of LC3B II as a measure of autophagic flux. Following Baf-A1 treatment, LC3B-II and p62 levels, two key markers of autophagy activity, increased continuously upon NR1D1 inhibition, indicating enhanced autophagic flux and basal level of macro-autophagy. As NR1D1 levels decreased, the protein level of LC3B-II was upregulated to varying degrees, indicating autophagy activation. Furthermore, we observed that reduced NR1D1 expression correlated with decreased cell viability, suggesting that excessive autophagy activation may lead to cell death (Fig. 1D; Supplementary Fig. 1G).

To further validate our findings, we used U2OS cells stably expressing protein, tandem fluorescent-tagged LC3 (ptf-LC3B), expressing a fluorescent tagged LC3B (mRFP-EGFP-LC3B) construct that enables monitoring of autophagic activity by detecting the fluorescence shift from yellow (both signals) to red fluorescence [29]. At neutral pH, autophagosomes display both red and green fluorescence due to the cytosolic localization of LC3B tagged with mRFP and EGFP (appearing as yellow puncta) (Fig. 1E). When autophagosomes fuse with the lysosomes to form autolysosomes, the pH drops. Acidic pH quenches the EGFP signal, and red-only signal therefore corresponds to LC3B within the autolysosomes (Fig. 1E). Starvation is known to induce autophagy. Therefore, we starved the cells for 2 hours with Earle's Balanced Salt Solution (EBSS) as a positive control for autophagy induction. In addition, we treated the cells with Baf-A1 to inhibit lysosomal acidification and autophagosome-lysosome fusion and hereby enabling the detection of autophagic flux (Fig. 1F–H). Our results showed that regardless of Baf-A1 treatment, the number of LC3B puncta with both green and red fluorescence increased significantly, and even more than in response to starvation. When quantifying the number of LC3B-red only puncta, exemplifying autophagolysosomes, *NR1D1* knockdown cells showed more red-only puncta than controls, and fewer than following starvation. Based on this finding of increased autophagosomes, but no change in autophagolysosomes, we speculated whether NR1D1 might affect the lysosomal activity or acidity. To determine the effect of NR1D1 deficiency on lysosomal function we stained the cells with LysoTracker (Supplementary Fig. 1H, I). LysoTracker is a fluorescent dye that entries cell membranes and accumulates in low

pH environments, specifically labeling lysosomes in live cells [30]. We found that NR1D1 deficiency did not affect the number of lysosomes detected with LysoTracker in either U2OS cells or YPH cells.

In conclusion, our findings demonstrate that NR1D1 inhibition enhances autophagic flux and autophagosome formation but does not impair lysosomal function.

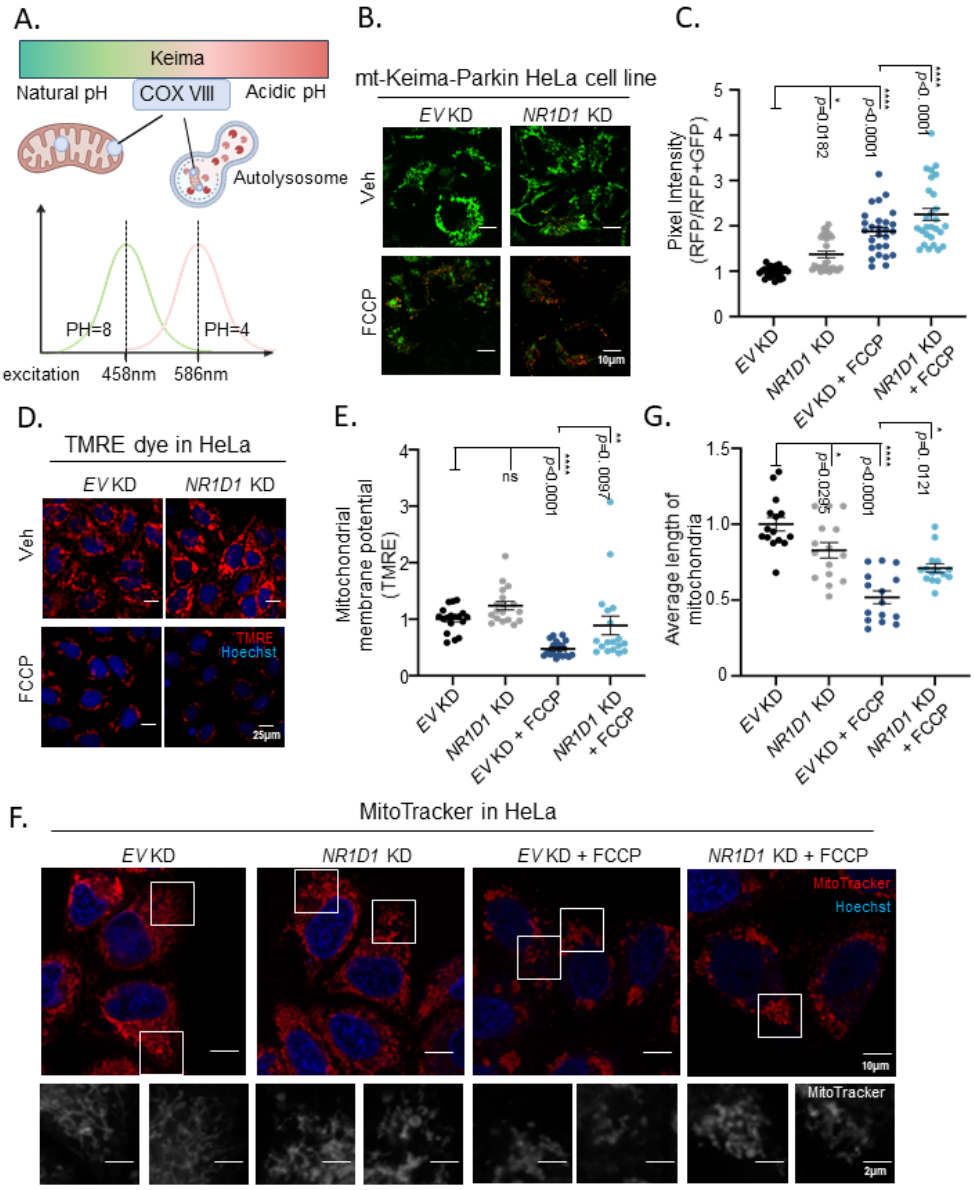

Figure 2. Activation of Mitophagy Following *NR1D1* Knockdown. (A) Schematic representation of the mt-Keima reporter system for monitoring mitophagy, indicating the fluorescence shift from GFP (natural pH) to RFP (acidic pH) in mitochondria entering autolysosomes. **(B, C)** Representative images and quantification of mt-Keima YPH cells treated with *EV* or *NR1D1* knockdown in the presence of vehicle (Veh) or FCCP. Data are pooled from 3 biological replicates and each repeat contains 9 pictures per group (n=27). **(D, E)** Representative images and quantification of TMRE staining in HeLa cells treated with *EV* or *NR1D1* KD, with or without FCCP, to assess mitochondrial membrane potential changes. Data are pooled from 3 biological replicates and each repeat contains 6 technical repeats (n=18). **(F, G)** Representative images and mitochondrial length quantification of MitoTracker staining in HeLa cells with *NR1D1* KD and corresponding controls to assess mitochondrial distribution and morphology. Data are pooled from 2 biological replicates and each repeat contains 8 pictures per group(n=16). Kruskal–Wallis test with Dunn's multiple comparison test (C, E, G) was performed for statistical analysis, with significance levels denoted as: ns = not significant, * $p < 0.05$, ** $p < 0.01$, *** $p < 0.001$, **** $p < 0.0001$. Data are presented as mean ± SEM.

Activation of Mitophagy Following *NR1D1* Knockdown

Mitophagy plays a crucial role in maintaining mitochondrial quality control due to its involvement in numerous diseases and mitochondria-related processes [21, 31]. In this study, we aimed to further examine the relationship between NR1D1, mitophagy, and mitochondrial homeostasis. First, we used HeLa cells expressing mitochondrial target Keima (mtKeima) and Parkin. mtKeima is a pH-sensitive fluorescent protein detecting the pH statement of mitochondrial matrix, using a mitochondrial targeting sequence from COX VIII. mtKeima serves as a precise indicator of mitophagy by detecting the delivery of mitochondria to acidic lysosomes for degradation [32] (Fig. 2A). mtKeima's excitation wavelength shifts from 458 nm at neutral pH to 586 nm in acidic conditions. While its emission wavelength remains constant at 620 nm, the fluorescence displayed will also change [32]. We applied Carbonyl cyanide-p-trifluoromethoxyphenylhydrazone (FCCP), a mitochondrial uncoupler that decreases mitochondrial membrane potential, to stimulate mitophagy. The results revealed that *NR1D1* knockdown enhanced mitophagy both in basal and FCCP-stimulated conditions (Fig. 2B). Since mitophagy has an essential role in mitochondrial homeostasis, we assessed mitochondrial membrane potential using Tetramethylrhodamine, ethyl ester (TMRE) staining, a fluorescent probe that will enter the mitochondria dependent on the membrane potential. We found that knockdown of *NR1D1* upregulated mitochondrial membrane potential under FCCP stimulation. Mitochondrial morphology analysis using MitoTracker revealed that *NR1D1* knockdown alone induced mitochondrial fragmentation, potentially due to hyper-activated mitophagy. We speculate that excessive mitophagy may promote mitochondrial fission through the enhanced degradation of mitochondria [31]. Additionally, NR1D1 acts as a nuclear receptor that inhibits the function of DRP1, a key regulator of mitochondrial fission. Inhibition of NR1D1 may activate DRP1 [33], thereby further promoting mitochondrial fission. However, during FCCP treatment, *NR1D1* knockdown improved mitochondrial morphology. We propose that under FCCP treatment, the number of damaged mitochondria increases, and the activation of mitophagy increased the recycling of damaged organelles. Our results demonstrate that *NR1D1* knockdown enhances mitophagy, contributing to improved mitochondrial homeostasis by promoting mitochondrial recycling and maintaining mitochondrial membrane potential. These findings highlight NR1D1 as a potential regulator of mitophagy.

NR1D1 Inhibition Enhances Autophagic Flux via SIRT1 and Cathepsin B

To explore the mechanism by which NR1D1 regulates autophagy, we first utilized the STRING database to predict protein-protein interactions between NR1D1 and autophagy-related proteins (Fig. 3A; Supplementary Table 1) (https://string-db.org/). Among these, we focused on the five autophagy-related proteins showing the strongest correlation with NR1D1 (HSP90AB1, SIRT1, ATG5, NAMPT, GAPDH). Additionally, our analysis of a previous study examining the effects of *NR1D1* knockout in U2OS cells (GSE248721) revealed that autophagy-related genes were altered (Fig. 3B; Fig. S2. A; Supplementary Table 2). Western blot analysis was performed on YPH cell extracts following *NR1D1* knockdown, with and without Baf-A1 treatment, to examine the five autophagy-proteins along with additional key autophagy markers (Fig. 3C). Our results revealed that *NR1D1* knockdown significantly increased the expression of Sirtuin 1 (SIRT1) and pro-CTSB cathepsin B (Cathepsin B) (Fig. 3D, E; Supplementaay Fig. 2B-L). SIRT1 promotes autophagy mainly by deacetylating and activating key autophagy-related proteins [34, 35]. Cathepsin B contributes to autophagy by degrading autophagic cargo within lysosomes, ensuring the efficient recycling of cellular components [36]. Under normal lysosomal conditions, the propeptide of Cathepsin B undergoes hydrolysis through either self-cleavage or processing by other proteases, resulting in the formation of mature, active cathepsin B [37]. Our results demonstrate that *NR1D1* knockdown significantly increases the expression of pro-Cathepsin B, but does not affect the levels of cleaved (active) Cathepsin B. These findings suggest that *NR1D1* KD specifically promotes the accumulation of pro-Cathepsin B without influencing its maturation into the active form. This data indicates that inhibition of NR1D1 may regulate autophagy by modulating SIRT1. Through computational protein interaction analysis and experimental validation, we identified SIRT1 and Cathepsin B as potential key molecular mediators between NR1D1 inhibition and autophagy.

Impact of NR1D1 Inhibition on Autophagy and Mitophagy in AD

From the above experiments, we showed that NR1D1 regulates autophagy. Building on these findings, we aim to examine the changes in NR1D1 expression during the progression of AD [14]. Differential expression analysis was conducted to investigate the role of NR1D1 in AD using human data from the Religious Orders Study and Memory and Aging Project (ROSMAP) [38, 39]. *NR1D1*

expression increased differently across all three comparisons with AD progression (Fig. 4A). The most pronounced differential expression was observed in Cut-Like Homeobox 2 (CUX2)+ cells, as highlighted by the rhombus symbol coverage. CUX2 is commonly used as a marker for upper-layer excitatory neurons [40]. The marked upregulation of NR1D1 in this context suggested a likely pivotal role of NR1D1 in the early stages of pathologies, particularly associated with the neurodegenerative changes characteristic of AD. These findings support the hypothesis that NR1D1 KD could serve as a potential therapy target.

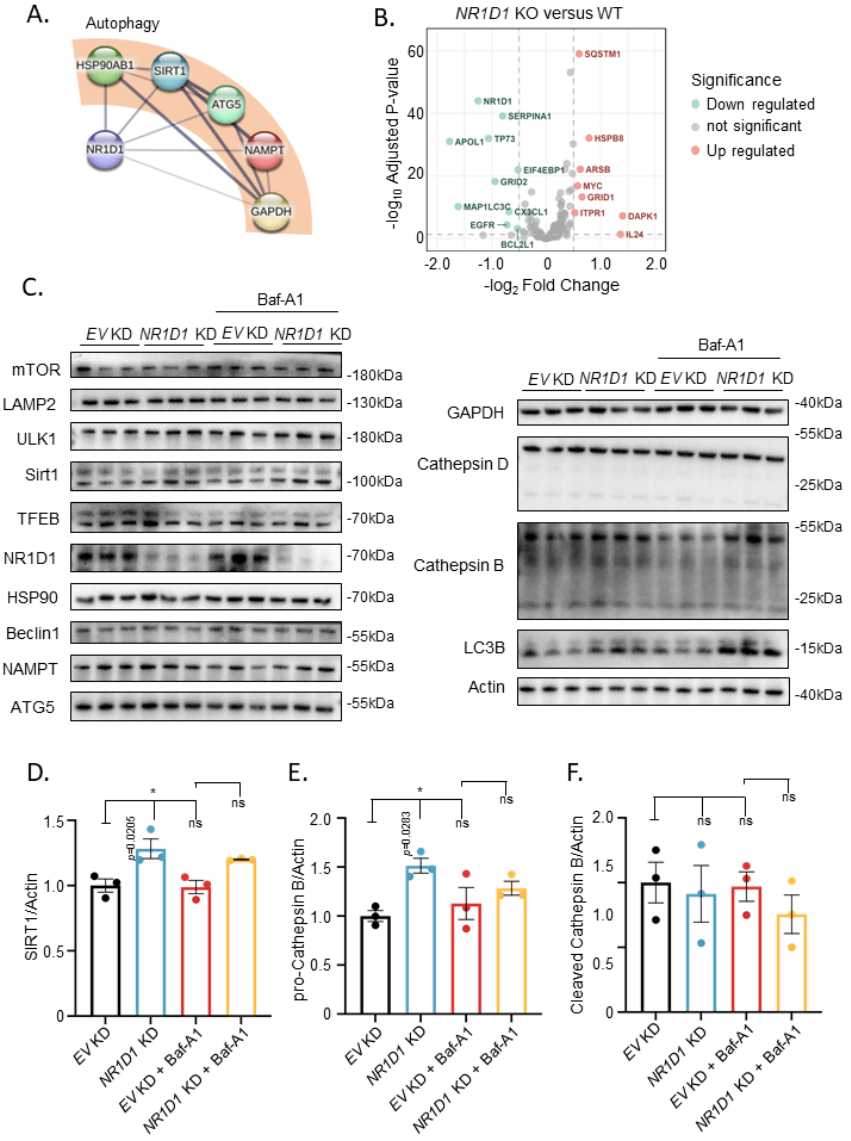

Figure 3. *NR1D1* Knockdown Activates Both Mitophagy and Autophagy via SIRT1. (A) Network diagram showing key protein interactions in autophagy regulation, emphasizing SIRT1 and related factors in response to *NR1D1* knockdown from STRING website. **(B)** Volcano plot showing differentially expressed genes (DEGs) related to autophagy in *Nr1d1* KO mice compared to wild types (absolute fold change > 0.5, adjusted *p* value < 0.05). Red indicates significantly upregulated genes, and green indicates significantly downregulated genes. **(C)** Western blot analysis of various autophagy and mitophagy-related proteins, including mTOR, LAMP2, ULK1, Sirt1, TFEB, NR1D1, HSP90, Beclin1, NAMPT, ATG5, Cathepsin D, Cathepsin B, LC3B, and GAPDH, in cells treated with *EV* or 20nM *NR1D1* siRNA in the presence or absence of Baf-A1. Data are pooled from 3 biological replicates (n=3). **(D, E)** Quantification of SIRT1, Cathepsin B and cleaved Cathepsin B levels in cells treated with *EV*, *NR1D1* KD, and Baf-A1, showing the impact of *NR1D1* knockdown. Two-way with Tukey's multiple comparison test (D, E, F) was performed for statistical analysis, with significance levels indicated as follows: ns = not significant, * $p < 0.05$, ** $p < 0.01$, *** $p < 0.001$, **** $p < 0.0001$. Data are presented as mean ± SEM.

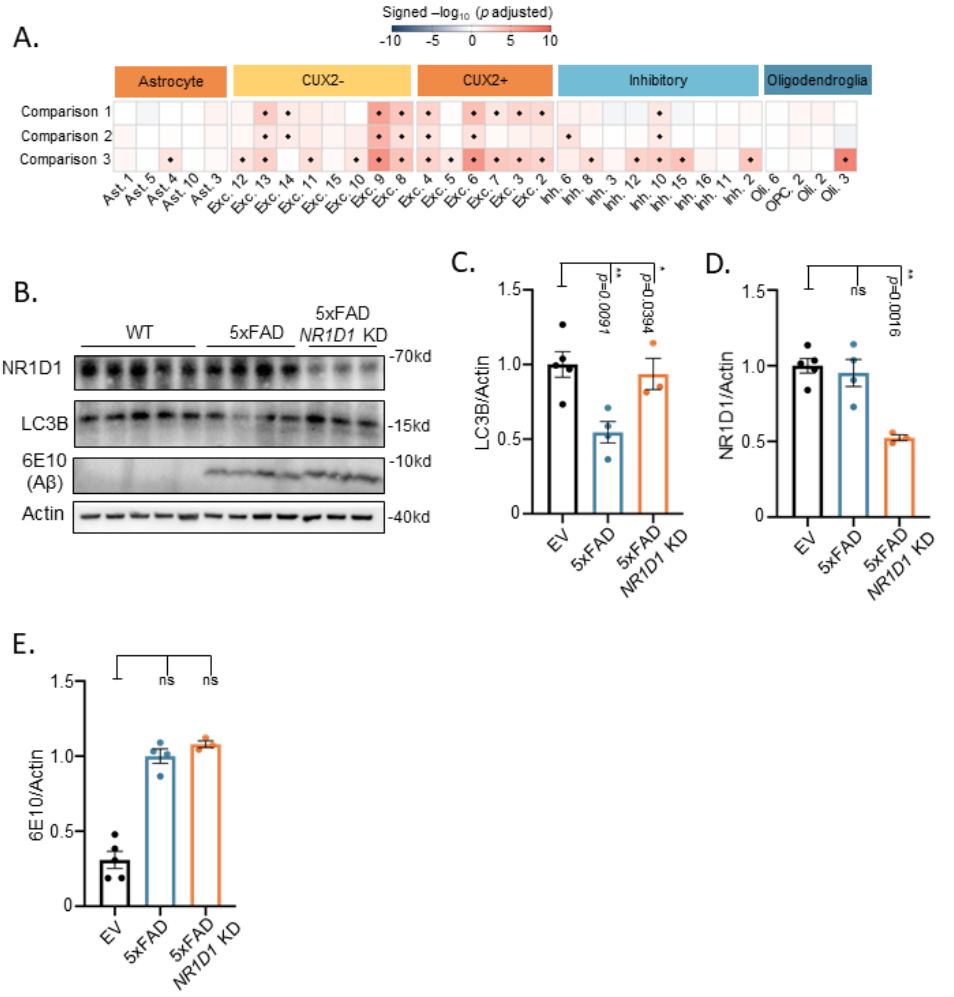

Figure 4. Impact of *NR1D1* Knockdown on Autophagy in AD. (A) Heat map showing the change of *NR1D1* in different comparisons of transcriptional changes in human PFC across five major brain neuron types, including astrocyte, CUX2- excitatory neuron, CUX2+ excitatory neuron, inhibitory neuron and Oligodendroglia. Comparison 1: Pathologic AD positive with AD-related dementia versus Pathologic AD negative without AD-related dementia; Comparison 2: Pathologic AD positive without AD-related dementia versus Pathologic AD negative without AD-related dementia; Comparison 3: Pathologic AD positive with AD-related dementia versus Pathologic AD negative with AD-related dementia. **(B)** Western blot analysis of various autophagy-related proteins in the hippocampus tissues, including NR1D1, LC3B and Actin, in WT and 5xFAD mice treated with hippocampal *EV* or *Nr1d1* knockdown. Data are pooled from 3-5 mice per group (n=3-5). **(C-E)** Quantification of SIRT1, NR1D1, 6E10 (Aβ) levels in WT and 5xFAD mice treated with EV or *Nr1d1* knockdown. One-way with Tukey's multiple comparison test was performed for statistical analysis, with significance levels indicated as follows: ns = not significant, * $p < 0.05$, ** $p < 0.01$, *** $p < 0.001$, **** $p < 0.0001$. Data are presented as mean ± SEM.

Since autophagy is impaired in AD, we aimed to determine whether we can restore the impairment through changes in NR1D1. We applied 5xFAD mice, which contain five AD-linked mutations: three in the APP695 gene [APP K670N/M671L (Swedish), I716V (Florida), V717I (London)] and two in the PSEN1 gene [M146L, L286V] [41]. We injected adeno-associated virus (AAV) encoding shRNA against *Nr1d1* (shRNA *Nr1d1*) and empty vector into the hippocampus of mice via stereotaxic injection. After 2 months, we collected the tissue and confirmed approx. 50% decrease of NR1D1 with western blotting. We also detected decreased LC3B expression in AD mice, subsequently restored following *Nr1d1* knockdown (Fig. 4B-D). However, in our detection, soluble Aβ did not change following *Nr1d1* knockdown (Fig. 4B, E).

nhr-85/NR1D1 Inhibition Enhances Neuronal Mitophagy, Restores Memory Deficits, and Extends Lifespan in AD *C. elegans* Models

We utilized Caenorhabditis elegans (*C. elegans*), a well-characterized nematode with a sophisticated nervous system [42], to investigate neuronal mitophagy mediated by *nhr-85* (*NR1D1* ortholog) *in vivo*. First, we used transgenic nematodes with pan-neuronal expression of mitochondria-targeted Rosella (mt-Rosella, a dual color-emission biosensor). The mt-Rosella biosensor comprises a green fluorescent protein (GFP) variant sensitive to the acidic environment of the lysosomal lumen, which is fused to the fast-maturing pH-insensitive DsRed. Mitophagy index is assessed by monitoring the GFP/DsRed ratio, with reduced values signifying mitophagy induction [43] (Fig. 5A). We knocked down *nhr-85* expression in the neurons of mtRosella nematodes using either *nhr-85* RNAi or an empty vector, under treatment with rotenone (a strong inhibitor of mitochondrial complex I and mitophagy inducer) or vehicle control. We then detected the fluorescence in the neurons of the tail region (Fig. 5B-D). Our results indicated that inhibition of *nhr-85* in nematodes promoted the occurrence of mitophagy with or without stress.

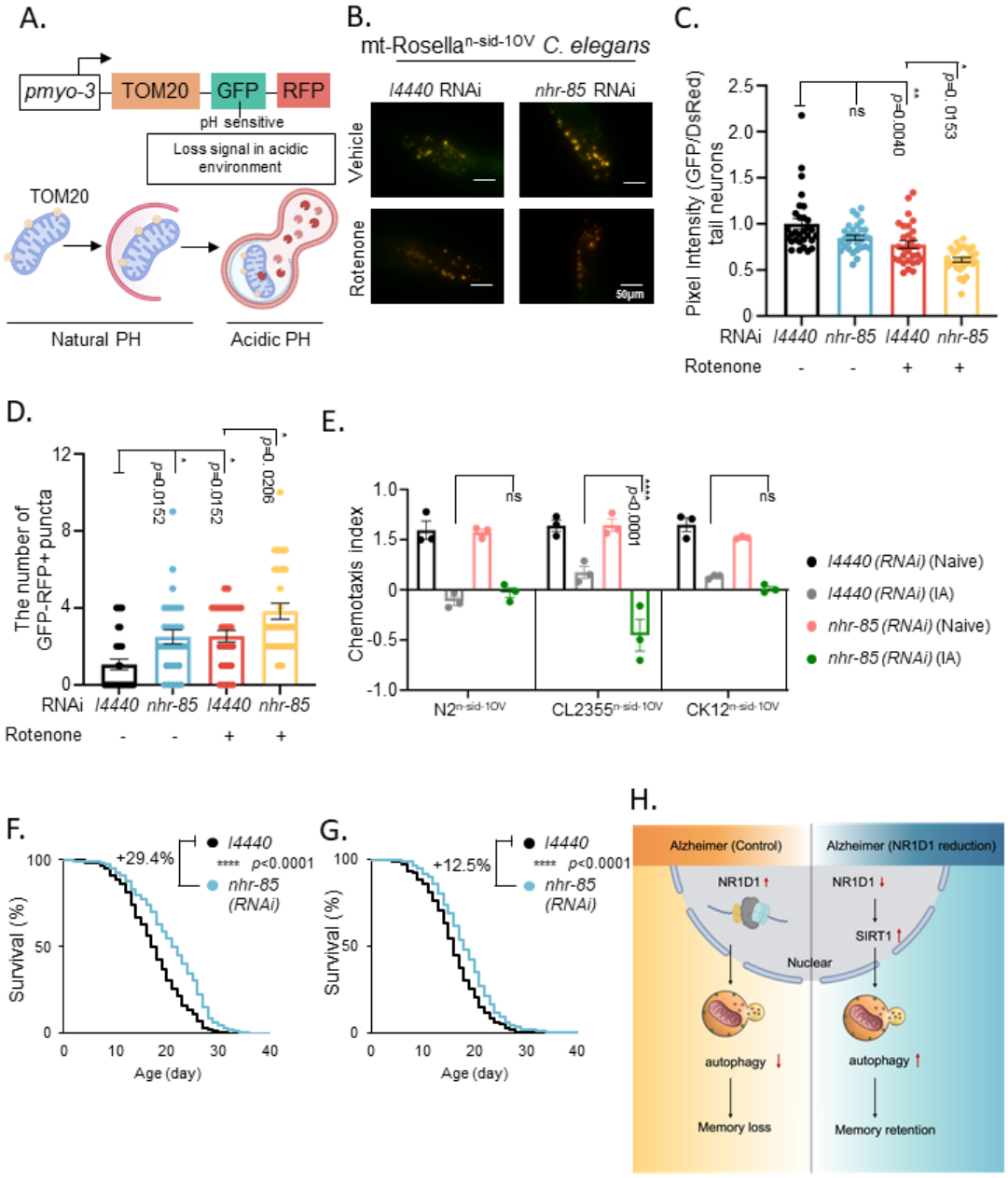

Figure 5. *NR1D1/nhr-85* Knockdown Provides Neuroprotection Against AD on Lifespan and Healthspan. **(A)** Schematic representation of the mt-Rosella reporter system, illustrating pH-sensitive changes in mitochondrial fluorescence signal from GFP (natural pH) to RFP (acidic pH) following mitophagy. **(B)** Representative images of pan-neuronal mt-Rosella expressing *C.elegans* treated with vehicle or rotenone in the presence or absence of *l4440/EV* or *nhr-85/NR1D1* knockdown. Data are pooled from 3 biological replicates and around each repeat contains 10 worms (n=30). **(C, D)** Quantification of pixel intensity (GFP/RFP ratio) and GFP-RFP+ puncta in neurons expressing mt-Rosella treated with *l4440* or *nhr-85* RNAi and exposed to rotenone, indicating changes in mitochondrial degradation. **(E)** Chemotaxis index in $N2^{n\text{-}sid\text{-}1OV}$, $hA\beta_{1-42}$ /$CL2355^{n\text{-}sid\text{-}1OV}$ and hTau[P301L]/ $CK12^{n\text{-}sid\text{-}1OV}$ with *l4440* or *nhr-85* RNAi treatment, indicating changes in neuronal function and behavior. Data are pooled from 3 biological replicates and each repeat contains around 200 worms per group (n=3). **(F, G)** Survival curve of N2 $^{n\text{-}sid\text{-}1OV}$ worms and $hA\beta_{1-42}$/CL2355 $^{n\text{-}sid\text{-}1OV}$ worms treated with *l4440/EV* RNAi or *nhr-85 / NR1D1* RNAi, showing effects on lifespan. Data are pooled from 3 biological replicates and around 90 worms per biological repeats per group (n=3). **(H)** The image compares the effects of Alzheimer's disease (control) and the knockdown of the *NR1D1* gene in Alzheimer's disease on key processes. In AD, NR1D1 is elevated, leading to decreased autophagy, resulting in memory loss. In contrast, the reduction of NR1D1 increases SIRT1, enhances autophagy and promotes memory retention. Kruskal–Wallis test with Dunn's multiple comparison test (C, D), Two-way ANOVA with Tukey's multiple comparison test (E) and simple survival analysis: Kaplan–Meier estimator (F, G) were performed statistical analysis, with significance levels indicated as follows: ns = not significant, * $p < 0.05$, ** $p < 0.01$, *** $p < 0.001$, **** $p < 0.0001$. Data are presented as mean ± SEM.

Given the causative role of compromised mitophagy in AD pathogenesis, we examined the impact of *nhr-85* on memory in both Aβ and tau nematode models. To investigate whether *nhr-85* inhibition restored memory deficits, we evaluated learning behavior in transgenic nematodes expressing pan-neuronal human $A\beta_{1-42}$ ($hA\beta_{1-42}$) or hTau4R1N(P301L) using an aversive olfactory learning chemotaxis assay, where a negative value correlates with chemotaxis-related memory [44] (Fig. 5 E). $hA\beta_{1-42}$ nematodes with *nhr-85* knockdown showed improved behavioral performance, whereas hTau4R1N(P301L) worms did not demonstrate restored associative memory upon *nhr-85* knockdown. These findings suggest that *nhr-85* inhibition can stimulate mitophagy in human cells and *C. elegans* neurons, particularly improving associative memory in $hA\beta_{1-42}$ transgenic worms. For tau worms, although autophagy was downregulated in the tau model [45] and *nhr-85* knockdown did activate autophagy, *nhr-85* knockdown did not improve chemotaxis-related memory in tau-expressing worms. This lack of improvement may stem from fundamental differences between the tau and Aβ models. Specifically, in murine models, tau acetylation [46], which contributed to memory impairment might be increased by *nhr-85/NR1D1* knockdown, since the inhibition of *nhr-85/NR1D1* could increase the tau acetylation [47]. Since population studies have demonstrated reduced lifespans among individuals with AD compared to healthy controls [48], we investigated whether enhanced memory correlated with increased longevity. Inhibition of *nhr-85* extended the average lifespan of WT worms and worms expressing $hA\beta_{1-42}$ by 29.4% and 12.5%, respectively (Fig. 5F, G; Table 2).

Overall, the results demonstrate that inhibition of *nhr-85* enhanced neuronal mitophagy, improved associative memory in $hA\beta_{1-42}$ transgenic *C. elegans*, and extended lifespan, suggesting that targeting *nhr-85* could offer a potential therapeutic strategy for AD.

Table 1. Statistical analysis of *C. elegans* lifespan data.

Fig	Strain, treatment	Mean lifespan (day ± SEM)	Median lifespan (day)	Median lifespan changes against EV
5F	N2; $(l4440\ RNAi)^{n\text{-}sid\text{-}1OV}$	17.55 ± 0.34	17	/
5F	N2; $(nhr\text{-}85\ RNAi)^{n\text{-}sid\text{-}1OV}$	20.85 ± 0.38	22	29.4%
5G	$hA\beta_{1-42}$;$(l4440\ RNAi)^{n\text{-}sid\text{-}1OV}$	16.09 ± 0.29	16	/
5G	$hA\beta_{1-42}$; $(nhr\text{-}85\ RNAi)^{n\text{-}sid\text{-}1OV}$	18.26 ± 0.31	18	12.5%

Survival analysis of N2 $^{n\text{-}sid\text{-}1OV}$ worms and $hA\beta_{1-42}$ (CL2355) $^{n\text{-}sid\text{-}1OV}$ worms treated with *l444 /Empty Vector* (*EV*) RNAi or *nhr-85 / NR1D1* RNAi, showing effects on lifespan. Data are pooled from 3 biological replicates and 90 worms per biological repeats.

DISCUSSION

Our study provides compelling evidence that NR1D1 serves as a crucial regulator of autophagy, with significant implications for understanding and potentially treating diseases characterized by autophagy dysfunction, such as AD. By demonstrating the potential of NR1D1 depletion to enhance autophagic flux, improve mitophagy, and potentially mitigate age-related neurological decline, we have demonstrated a promising avenue for future

therapeutic interventions. The multi-species approach, utilizing cell lines, mouse models, and *C. elegans*, strengthens the robustness of our findings and highlights the conserved nature of the role of NR1D1 in autophagy regulation across different biological systems. While further research is needed to fully elucidate the molecular mechanisms and potential clinical applications, our work provides a solid foundation for future studies targeting NR1D1 as a potential therapeutic strategy for autophagy-related disorders.

Despite these promising results, several critical questions remain unanswered and warrant further investigation. Notably, in this study, we used Western blot analysis to demonstrate that NR1D1 inhibition does not affect soluble Aβ levels. While NR1D1 depletion does not reduce soluble Aβ, it might increase cellular/neuronal resilience against internal and external stresses via other approaches. This could be via enhanced cellular metabolism and reduction of cell death signaling: these hypotheses should be tested in cellular and animal models in future studies. Our data do not exclude the possibility of changes in $A\beta_{1-42}$, APP, and CTF of APP by NR1D1 reduction in other cellular or animal models of AD. In our study, *NR1D1* knockdown was shown to activate autophagy through multiple approaches, including the mCherry-GFP-LC3 reporter cell line, LysoTracker staining, and western blotting. Despite this activation, we observed increased p62 levels, which could be explained by several mechanisms. First, autophagy flux might be impaired at a late stage, such as lysosomal fusion or degradation, although LysoTracker staining indicated normal lysosomal function. Second, as a nuclear transcription factor regulated by HDAC3, NR1D1 may influence p62 expression through autophagy-independent pathways, such as NRF2-mediated stress responses, or by affecting cellular stress signaling and the ubiquitin-proteasome system (UPS), potentially leading to increased p62 levels. Meanwhile, the relationship between NR1D1 and SIRT1 remains ambiguous. While SIRT1 is known to regulate NR1D1 through the management of BMAL1 [49, 50], the reciprocal effects of NR1D1 on SIRT1 activity and function require elucidation. Additionally, comprehensive studies are needed to determine whether the benefits of *NR1D1* KD are directly dependent on SIRT1 activation or if there are alternative mechanisms at play. Cathepsin B is localized not only in lysosomes but also in the nucleus and other cytoplasmic regions [51]. Furthermore, LysoTracker staining results and the cleaved Cathepsin B remained unchanged, indicating that the specific cellular compartments in which Cathepsin B levels increase upon *NR1D1* knockdown maybe except lysosome. NR1D1 is known to influence gene expression through transcriptional regulation and modulate protein function via deacetylation. Further studies are required to investigate whether NR1D1 directly affects cathepsin B at the transcriptional level, post-translationally through deacetylation [52, 53], or through other indirect pathways. Identifying the downstream pathways between NR1D1 and autophagy regulation could further enhance our ability to exploit this axis for therapeutic gain. Exploring these nuanced interactions will be crucial in targeting NR1D1 in therapeutic strategies. Like a double-edged sword, it is noteworthy that NR1D1 has both positive and negative effects to the cells. Under physiological condition, cellular processes such as autophagy and *NR1D1* knockdown induce excessive autophagy, ultimately causing cell death; in Alzheimer's disease, insufficient autophagy plays a key pathological role and NR1D1 helps maintain mitochondrial integrity under conditions of mitochondrial damage. In this study, *NR1D1* (*nhr-85* in *C. elegans*) KD improved cellular homeostasis, healthspan and lifespan in AD worms; however, we do not exclude any potential side effects caused by *NR1D1* KD. Further experiments on any side effects by *NR1D1* KD should be carried out before applying this strategy for AD therapy.

The research reveals that targeting NR1D1 KD can restore impaired autophagy, as evidenced by our findings in both cellular models and animal studies, including *C. elegans* and 5xFAD mice. Notably, the *nhr-85* KD not only improved mitophagy but also showed potential in extending lifespan and improving memory in AD models. This suggests that NR1D1 depletion could be a valuable therapeutic target for neurodegenerative disorders where autophagy and mitochondrial function are compromised.

Acknowledgements

This project was supported by Cure Alzheimer's Fund (#282952), HELSE SØR-ØST (#2020001, #2021021, #2023093), International collaborative research project of Shenzhen Science and Technology Plan (GJHZ 20210705142008027), the Research Council of Norway (#262175, #334361), NordForsk Foundation (#119986), the National Natural Science Foundation of China (#81971327), Akershus University Hospital (#269901, #261973, #262960), the Civitan Norges Forskningsfond for Alzheimers sykdom (#281931), the Czech Republic-Norway KAPPA programme (with Martin Vyhnálek, #TO01000215) to EFF; EFF is also supported by the Rosa sløyfe/Norwegian Cancer Society & Norwegian Breast Cancer Society (#207819) and Molecule AG/VITADAO (#282942); Guang Yang was supported in part by the ERC IMI (101005122), the H2020 (952172), the MRC (MC/PC/21013), the Royal Society (IEC\NSFC\211235), the NVIDIA Academic Hardware Grant Program, the SABER project supported by Boehringer Ingelheim Ltd,

NIHR Imperial Biomedical Research Centre (RDA01), Wellcome Leap Dynamic Resilience, UKRI guarantee funding for Horizon Europe MSCA Postdoctoral Fellowships (EP/Z002206/1), and the UKRI Future Leaders Fellowship (MR/V023799/1). Sofie Lautrup is supported by The Norwegian Health Association. Shi-qi Zhang is supported by China Scholarship Council (#202008210272), HSØ midler (#270921), Ahus University Hospital Tildeling av Interne Forskningsmidler for 2024.

The bioinformatic results published from the Religious Orders Study and Rush Memory and Aging Project (ROSMAP) database are in whole or in part based on data obtained from the AD Knowledge Portal (https://adknowledgeportal.org). We thank and acknowledge the individuals and their family members of the ROSMAP study. Study data were generated from post-mortem brain tissue provided by the ROSMAP cohort at Rush Alzheimer's Disease Center, Rush University Medical Center, Chicago. This work was funded by NIH grants U01AG061356 (De Jager/Bennett), RF1AG057473 (De Jager/Bennett), and U01AG046152 (De Jager/Bennett) as part of the AMP-AD consortium, as well as NIH grants R01AG066831 (Menon) and U01AG072572 (De Jager/St George-Hyslop).

Conflict of Interest

E.F.F. is a co-owner of Fang-S Consultation AS (Organization number 931 410 717) and NO-Age AS (Organization number 933 219 127); he has an MTA with LMITO Therapeutics Inc (South Korea), a CRADA arrangement with ChromaDex (USA), a commercialization agreement with Molecule AG/ VITADAO, and MTAs with GeneHarbor (Hong Kong) Biotechnologies Limited and Hong Kong Longevity Science Laboratory (Hong Kong); he is a consultant to MindRank AI (China), NYO3 (Norway), and AgeLab (Vitality Nordic AS, Norway).

Supplementary Materials

The Supplementary data can be found online at: www.aginganddisease.org/EN/10.14336/AD.2024.1654.

References

[1] Bugge A, Feng D, Everett LJ, Briggs ER, Mullican SE, Wang F, et al. (2012). Rev-erbα and Rev-erbβ coordinately protect the circadian clock and normal metabolic function. Genes Dev, 26:657-667.

[2] Everett LJ, Lazar MA (2014). Nuclear receptor Rev-erbα: up, down, and all around. Trends Endocrinol Metab, 25:586-592.

[3] Preitner N, Damiola F, Lopez-Molina L, Zakany J, Duboule D, Albrecht U, Schibler U (2002). The orphan nuclear receptor REV-ERBalpha controls circadian transcription within the positive limb of the mammalian circadian oscillator. Cell, 110:251-260.

[4] Duez H, Staels B (2009). Rev-erb-alpha: an integrator of circadian rhythms and metabolism. J Appl Physiol (1985), 107:1972-1980.

[5] Solt LA, Wang Y, Banerjee S, Hughes T, Kojetin DJ, Lundasen T, et al. (2012). Regulation of circadian behaviour and metabolism by synthetic REV-ERB agonists. Nature, 485:62-68.

[6] Liu H, Zhu Y, Gao Y, Qi D, Zhao L, Zhao L, et al. (2020). NR1D1 modulates synovial inflammation and bone destruction in rheumatoid arthritis. Cell Death Dis, 11:129.

[7] Kim SM, Jeon Y, Jang JY, Lee H (2023). NR1D1 deficiency in the tumor microenvironment promotes lung tumor development by activating the NLRP3 inflammasome. Cell Death Discov, 9:278.

[8] Chandra V, Bhagyaraj E, Nanduri R, Ahuja N, Gupta P (2015). NR1D1 ameliorates Mycobacterium tuberculosis clearance through regulation of autophagy. Autophagy, 11:1987-1997.

[9] Woldt E, Sebti Y, Solt LA, Duhem C, Lancel S, Eeckhoute J, et al. (2013). Rev-erb-α modulates skeletal muscle oxidative capacity by regulating mitochondrial biogenesis and autophagy. Nat Med, 19:1039-1046.

[10] Chen Y, Li J, Li S, Cheng Y, Fu X, Li J, Zhu L (2023). Uncovering the Novel Role of NR1D1 in Regulating BNIP3-Mediated Mitophagy in Ulcerative Colitis. Int J Mol Sci, 24.

[11] Sulli G, Rommel A, Wang X, Kolar MJ, Puca F, Saghatelian A, et al. (2018). Pharmacological activation of REV-ERBs is lethal in cancer and oncogene-induced senescence. Nature, 553:351-355.

[12] DeTure MA, Dickson DW (2019). The neuropathological diagnosis of Alzheimer's disease. Mol Neurodegener, 14:32.

[13] Gilbert MAG, Fatima N, Jenkins J, O'Sullivan TJ, Schertel A, Halfon Y, et al. (2024). CryoET of β-amyloid and tau within postmortem Alzheimer's disease brain. Nature, 631:913-919.

[14] Lee JH, Yang DS, Goulbourne CN, Im E, Stavrides P, Pensalfini A, et al. (2022). Faulty autolysosome acidification in Alzheimer's disease mouse models induces autophagic build-up of Aβ in neurons, yielding senile plaques. Nat Neurosci, 25:688-701.

[15] Palmer JE, Wilson N, Son SM, Obrocki P, Wrobel L, Rob M, et al. (2024). Autophagy, aging, and age-related neurodegeneration. Neuron.

[16] Aman Y, Schmauck-Medina T, Hansen M, Morimoto RI, Simon AK, Bjedov I, et al. (2021). Autophagy in healthy aging and disease. Nat Aging, 1:634-650.

[17] Carosi JM, Hein LK, van den Hurk M, Adams R, Milky B, Singh S, et al. (2021). Retromer regulates the lysosomal clearance of MAPT/tau. Autophagy, 17:2217-2237.

[18] Wu S, Wei Y, Li J, Bai Y, Yin P, Wang S (2021). SIRT5 Represses Neurotrophic Pathways and Aβ Production in

Alzheimer's Disease by Targeting Autophagy. ACS Chem Neurosci, 12:4428-4437.

[19] Wang W, Zhao F, Ma X, Perry G, Zhu X (2020). Mitochondria dysfunction in the pathogenesis of Alzheimer's disease: recent advances. Mol Neurodegener, 15:30.

[20] Zong Y, Li H, Liao P, Chen L, Pan Y, Zheng Y, et al. (2024). Mitochondrial dysfunction: mechanisms and advances in therapy. Signal Transduct Target Ther, 9:124.

[21] Fang EF, Hou Y, Palikaras K, Adriaanse BA, Kerr JS, Yang B, et al. (2019). Mitophagy inhibits amyloid-β and tau pathology and reverses cognitive deficits in models of Alzheimer's disease. Nat Neurosci, 22:401-412.

[22] Xie C, Zhuang XX, Niu Z, Ai R, Lautrup S, Zheng S, et al. (2022). Amelioration of Alzheimer's disease pathology by mitophagy inducers identified via machine learning and a cross-species workflow. Nat Biomed Eng, 6:76-93.

[23] Cao SQ, Wang HL, Palikaras K, Tavernarakis N, Fang EF (2023). Chemotaxis assay for evaluation of memory-like behavior in wild-type and Alzheimer's-disease-like C. elegans models. STAR Protoc, 4:102250.

[24] Fang EF, Kassahun H, Croteau DL, Scheibye-Knudsen M, Marosi K, Lu H, et al. (2016). NAD(+) Replenishment Improves Lifespan and Healthspan in Ataxia Telangiectasia Models via Mitophagy and DNA Repair. Cell Metab, 24:566-581.

[25] Green GS, Fujita M, Yang HS, Taga M, Cain A, McCabe C, et al. (2024). Cellular communities reveal trajectories of brain ageing and Alzheimer's disease. Nature, 633:634-645.

[26] Huang G, Zhang F, Ye Q, Wang H (2016). The circadian clock regulates autophagy directly through the nuclear hormone receptor Nr1d1/Rev-erbα and indirectly via Cebpb/(C/ebpβ) in zebrafish. Autophagy, 12:1292-1309.

[27] Waters CS, Angenent SB, Altschuler SJ, Wu LF (2023). A PINK1 input threshold arises from positive feedback in the PINK1/Parkin mitophagy decision circuit. Cell Rep, 42:113260.

[28] Mauvezin C, Neufeld TP (2015). Bafilomycin A1 disrupts autophagic flux by inhibiting both V-ATPase-dependent acidification and Ca-P60A/SERCA-dependent autophagosome-lysosome fusion. Autophagy, 11:1437-1438.

[29] Kimura S, Noda T, Yoshimori T (2007). Dissection of the autophagosome maturation process by a novel reporter protein, tandem fluorescent-tagged LC3. Autophagy, 3:452-460.

[30] Huang K, Jiang X, Du J, Zeng H (2024). Protocol for detecting lysosome quantity and membrane permeability in acute myeloid leukemia cell lines. STAR Protoc, 5:103309.

[31] Wang S, Long H, Hou L, Feng B, Ma Z, Wu Y, et al. (2023). The mitophagy pathway and its implications in human diseases. Signal Transduct Target Ther, 8:304.

[32] Sun N, Malide D, Liu J, Rovira, II, Combs CA, Finkel T (2017). A fluorescence-based imaging method to measure in vitro and in vivo mitophagy using mt-Keima. Nat Protoc, 12:1576-1587.

[33] Pan Z, Yao Y, Liu X, Wang Y, Zhang X, Zha S, Hu K (2024). Nr1d1 inhibition mitigates intermittent hypoxia-induced pulmonary hypertension via Dusp1-mediated Erk1/2 deactivation and mitochondrial fission attenuation. Cell Death Discov, 10:459.

[34] Ding X, Zhu C, Wang W, Li M, Ma C, Gao B (2024). SIRT1 is a regulator of autophagy: Implications for the progression and treatment of myocardial ischemia-reperfusion. Pharmacol Res, 199:106957.

[35] Zhang M, Zhang Q, Hu Y, Xu L, Jiang Y, Zhang C, et al. (2017). miR-181a increases FoxO1 acetylation and promotes granulosa cell apoptosis via SIRT1 downregulation. Cell Death Dis, 8:e3088.

[36] Yim WW, Mizushima N (2020). Lysosome biology in autophagy. Cell Discov, 6:6.

[37] Mort JS, Buttle DJ (1997). Cathepsin B. Int J Biochem Cell Biol, 29:715-720.

[38] Bennett DA, Schneider JA, Buchman AS, Barnes LL, Boyle PA, Wilson RS (2012). Overview and findings from the rush Memory and Aging Project. Curr Alzheimer Res, 9:646-663.

[39] Bennett DA, Buchman AS, Boyle PA, Barnes LL, Wilson RS, Schneider JA (2018). Religious Orders Study and Rush Memory and Aging Project. J Alzheimers Dis, 64:S161-s189.

[40] Cubelos B, Sebastián-Serrano A, Beccari L, Calcagnotto ME, Cisneros E, Kim S, et al. (2010). Cux1 and Cux2 regulate dendritic branching, spine morphology, and synapses of the upper layer neurons of the cortex. Neuron, 66:523-535.

[41] Oakley H, Cole SL, Logan S, Maus E, Shao P, Craft J, et al. (2006). Intraneuronal beta-amyloid aggregates, neurodegeneration, and neuron loss in transgenic mice with five familial Alzheimer's disease mutations: potential factors in amyloid plaque formation. J Neurosci, 26:10129-10140.

[42] Roussos A, Kitopoulou K, Borbolis F, Palikaras K (2023). Caenorhabditis elegans as a Model System to Study Human Neurodegenerative Disorders. Biomolecules, 13.

[43] Palikaras K, Lionaki E, Tavernarakis N (2019). Mitophagy Dynamics in Caenorhabditis elegans. Methods Mol Biol, 1880:655-668.

[44] Voglis G, Tavernarakis N (2008). A synaptic DEG/ENaC ion channel mediates learning in C. elegans by facilitating dopamine signalling. Embo j, 27:3288-3299.

[45] Silva MC, Nandi GA, Tentarelli S, Gurrell IK, Jamier T, Lucente D, et al. (2020). Prolonged tau clearance and stress vulnerability rescue by pharmacological activation of autophagy in tauopathy neurons. Nat Commun, 11:3258.

[46] Cook C, Stankowski JN, Carlomagno Y, Stetler C, Petrucelli L (2014). Acetylation: a new key to unlock tau's role in neurodegeneration. Alzheimers Res Ther, 6:29.

[47] Alenghat T, Meyers K, Mullican SE, Leitner K, Adeniji-Adele A, Avila J, et al. (2008). Nuclear receptor corepressor and histone deacetylase 3 govern circadian metabolic physiology. Nature, 456:997-1000.

[48] Wolfson C, Wolfson DB, Asgharian M, M'Lan CE, Ostbye T, Rockwood K, Hogan DB (2001). A reevaluation of the duration of survival after the onset of dementia. N Engl J Med, 344:1111-1116.

[49] Belden WJ, Dunlap JC (2008). SIRT1 is a circadian deacetylase for core clock components. Cell, 134:212-214.

[50] Asher G, Gatfield D, Stratmann M, Reinke H, Dibner C, Kreppel F, et al. (2008). SIRT1 regulates circadian clock gene expression through PER2 deacetylation. Cell, 134:317-328.

[51] Cao F, Tang C, Chen X, Tu Z, Jin Y, Turk OM, et al. (2024). Cathepsin B Nuclear Flux in a DNA-Guided "Antinuclear Missile" Cancer Therapy. ACS Cent Sci, 10:1562-1572.

[52] Yin L, Lazar MA (2005). The orphan nuclear receptor Rev-erbalpha recruits the N-CoR/histone deacetylase 3 corepressor to regulate the circadian Bmal1 gene. Mol Endocrinol, 19:1452-1459.

[53] Kim YH, Marhon SA, Zhang Y, Steger DJ, Won KJ, Lazar MA (2018). Rev-erbα dynamically modulates chromatin looping to control circadian gene transcription. Science, 359:1274-1277.